Oxygen Incorporation into Si Nanocrystal/SiC Multilayers

Charlotte Weiss, Andreas Reichert, Johannes Hofmann, Stefan Janz

Fraunhofer Institute for Solar Energy Systems, Heidenhofstraße 2, 79110 Freiburg, Germany.

***Abstract* — We aimed to improve the properties of Si nanocrystal/SiC multilayers (ML) for the use as high bandgap solar cell absorber by the incorporation of oxygen (O). Therefore we compare the structural properties of Si nanocrystal/SiC ML with and without incorporated O by scanning electron microscopy, Raman spectroscopy and grazing incidence X-ray diffraction patterns. The O incorporation in the form of Si-O bonds was successful and a beneficial effect of O on the conservation of the ML structure during annealing and on the c-Si/c-SiC ratio is observed and discussed in detail.**

Keywords: Si nanocrystals, multilayer, SiC, Si tandem

I. Introduction

A solar cell (SC) with a bottom cell of conventional crystalline bulk Si (c-Si) and a top cell with a higher bandgap of silicon nanocrystals (NC) embedded in a dielectric matrix represents a potential material system for a crystalline Si tandem SC. The ideal bandgap for a top cell on a c-Si (1.1 eV) bottom cell was calculated to be 1.7 eV [1]. This can be achieved in Si with the help of the quantum confinement effect [2], which means enlarging the Si bandgap by reduction of the Si crystals to the nano-scale.

The use of 3C-SiC as a matrix material for Si NC is interesting as it provides a small conduction band offset of 0.5 eV compared with other typical matrix materials (1.9 eV for Si_3N_4 or 3.2 eV for SiO_2 [2]), with the same trend expected for the valence band. A small band offset increases the tunneling probability from one Si NC to the other and hence the conductivity of the material, making transport less sensitive to variations in NC separation [2, 3].

The so-called multilayer (ML) approach has been developed to reach Si NC size control for the adjustment of the Si bandgap. Alternating single layers (SL) of stoichiometric SiC barriers (SiC) and Si rich SiC wells (SRC) with thicknesses in the nm range are deposited. Typically the deposition is performed by plasma enhanced chemical vapor deposition (PECVD), followed by an annealing step at 1100°C by furnace anneal [4–6].

During the annealing step, phase separation and Si NC formation are expected to occur in the SRC layers while the SiC layers should serve as diffusion barrier. Furthermore, the annealing causes hydrogen (H) effusion as the films are usually deposited from the precursor gases SiH_4 and CH_4. The ML approach is known to work very well for Si NC size control in SiO_2 [7], but is much more challenging in SiC because interdiffusion of the SiC and the SRC layer occurs [4, 6]. In addition, co-crystallization of Si and SiC NC was observed and no clear evidence of quantum confinement was adduced due to the very weak photo-luminescence (PL) signal from Si_xC_{1-x} samples [6, 8, 9]. The absolute luminescence quantum yield of Si_xC_{1-x} samples was estimated by Schnabel *et al.* [10] to be very low ($<10^{-6}$), indicating a high density of non-radiative recombination-active defects, due to H effusion and co-crystallization during annealing [5]. The high defect densities must be strongly reduced in order to develop a good absorber material for SC.

This work proposes the incorporation of oxygen (O) into the Si NC/SiC ML as it is expected to (i) prevent the SiC crystallization to reduce the interfaces and stress in the material as reported by Kurokawa *et al.* [11], (ii) to passivate Si dangling bonds by the formation of Si-O bonds and (iii) to decrease the ML intermixing by behaving more like Si NC in SiO_2.

II. Experimental

Two types of substrates were used for layer deposition: (i) 250 µm thick p-doped float zone Si, (100)-oriented with a resistivity of 10 Ωcm. (ii) 1 mm thick fused silica (Suprasil®) substrates.

All ML and SL samples used in this work were deposited by PECVD conducted in a *Roth&Rau* AK400 reactor. The pressure during deposition was kept at 0.3 mbar and the substrate temperature at 270°C. The plasma power density was 100 mW/cm² at a frequency of 13.56 MHz. The variation of the gas fluxes of SiH_4, CH_4 and H_2 allows the deposition of hydrogenated a-SiC (a-Si_xC_{1-x}:H) with varying stoichiometry. After deposition, all samples were subjected to a furnace anneal step of 30 min@1100°C.

The samples on Si substrates were subsequently characterized by scanning electron microscopy (SEM), grazing incidence X-ray diffraction (GIXRD) and Fourier transformed infrared spectroscopy (FTIR) measurements. The samples on fused silica substrate were characterized by Raman spectroscopy.

In a first experiment, it was checked if the use of CO_2 as precursor gas leads to the desired O incorporation into the samples. Therefore, $Si_{0.50}C_{0.50}$ and $Si_{0.77}C_{0.23}$ SL were deposited under CO_2 fluxes varying between 0.0 and 10.0 sccm. To compensate a possible increase in C content in the samples due to the CO_2 flux, the CH_4 flux was reduced by the same amount as the CO_2 flux was increased. In a second experiment, the influence of O incorporation on ML stacks with 20 bilayers of $Si_{0.50}C_{0.50}/Si_{0.77}C_{0.23}$ (6 nm/9 nm) was examined. The choice of the sublayer thickness leads to an overall Si content of 63% and allows a direct comparison between ML and $Si_{0.63}C_{0.37}$ SL.

Three different types of ML and two different SL (≈ 200 nm) for comparison were prepared:

- ML without CO_2 **ML0**
- ML with CO_2 flux during $Si_{0.77}C_{0.23}$ sublayer deposition **ML77**
- ML with CO_2 flux during $Si_{0.50}C_{0.50}$ sublayer deposition **ML50**
- SL $Si_{0.63}C_{0.37}$ with CO_2 **SL63**
- SL $Si_{0.77}C_{0.23}$ with CO_2 **SL77**

III. RESULTS AND DISCUSSION

The FTIR spectra in Fig. 1 show that the increase in CO_2 flux from 0.0 to 10.0 sccm leads to an increased vibration mode

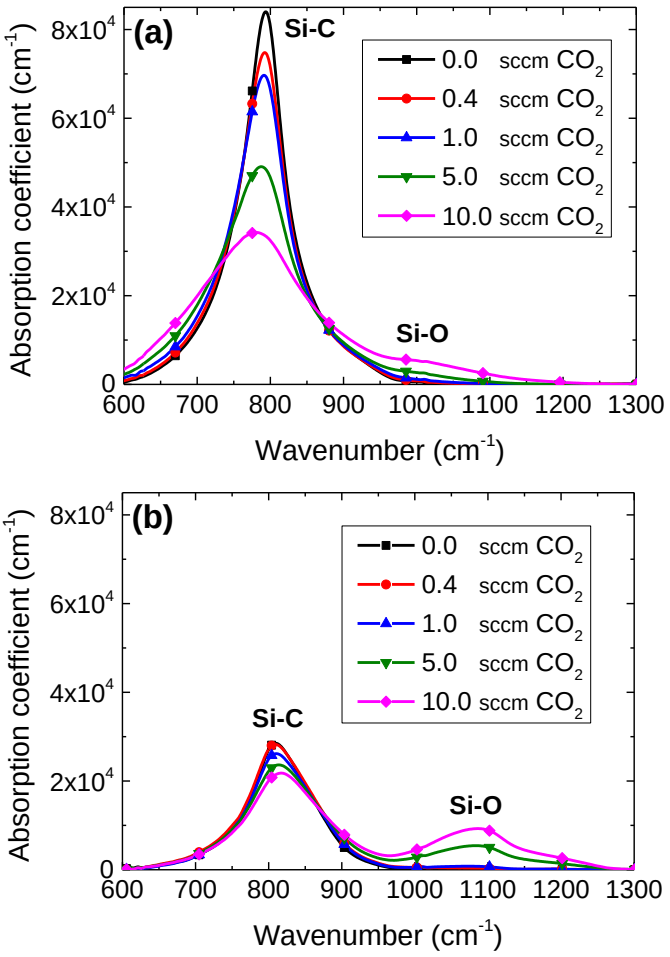

Fig. 1. FTIR spectra of (a) $Si_{0.50}C_{0.50}$ and (b) $Si_{0.77}C_{0.23}$ samples deposited with increasing amounts of CO_2 among the precursor gases and annealed for 30min@1100°C by furnace anneal. The increasing Si-O mode indicates the successful oxygen incorporation.

between 1000 and 1200 cm^{-1}. This result confirms the successful incorporation of O by CO_2 precursor gas as either Si-O or C-O vibrations are expected in this wavelength range [12]. The increase of the vibration mode related signal for a certain CO_2 flux is stronger in the case of $Si_{0.77}C_{0.23}$ (Fig. 1(b)) than in $Si_{0.50}C_{0.50}$ samples (Fig. 1(a)). Therefore, it is assigned to Si-O vibrations as an increasing Si-O bond density with increasing Si content seems more obvious than an increasing C-O content with increasing Si content. It can be concluded from the SL experiments that O incorporation into the samples by adding CO_2 to the precursor gases was successful.

As a second step, the O-containing SL were combined to ML. In Fig. 2, SEM cross sections of the ML before and after annealing at 1100°C are shown.

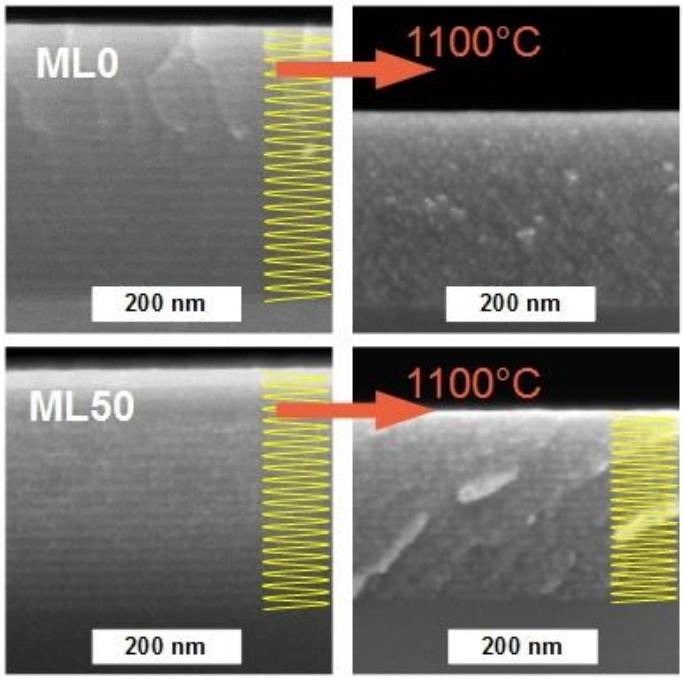

Fig. 2. SEM cross section images of ML deposited with and without CO_2 as precursor gas before and after annealing for 30min@1100°C by FA.

The ML with and without CO_2 show a layered structure in the SEM cross section before annealing. After annealing, the ML structure is lost in the ML0 samples as expected. However, in the case of ML with O, the ML structure is preserved during the annealing process as shown by the example of ML50 in Fig. 2. ML77 (not shown here) shows the same layered structure after annealing. For the first time, a ML structure with a Si content of only 77% in the Si-rich layers survived an annealing step of 30min@1100°C. It is concluded from this result that O in the samples hinders Si or C diffusion and therefore intermixing of the sublayers. FTIR spectra (not shown here) of as-deposited $Si_{0.50}C_{0.50}$ and $Si_{0.77}C_{0.23}$ samples prove the formation of Si-O bonds and show that approximately 60% of these bonds are already present after deposition. This is only a rough estimation as the Si-O vibration in the as-dep samples overlap strongly with the Si-H

vibration. However, the large amount of Si-O bonds present prior to annealing are probably responsible for the reduced Si and C mobility during the annealing step. This interpretation is supported by the Raman and GIXRD results presented in Fig. 3(a) and (b), respectively. All normalized Raman spectra are plotted in Fig. 3(a). The black (◆) and the green (■) spectra show SL63 and SL77, respectively. The brown (▲) spectrum represents ML0, and the orange (✳) and red (●) spectra represent the samples ML77 and ML50. Both ML have an overall Si content of 63%. The sample with the highest Si content (77%) clearly shows the most pronounced Raman c-Si peak (green spectra, ■) and a c-Si peak position at higher wavenumbers than the other spectra. This can be explained by a larger fraction of crystalline Si present in the SL77 than in the

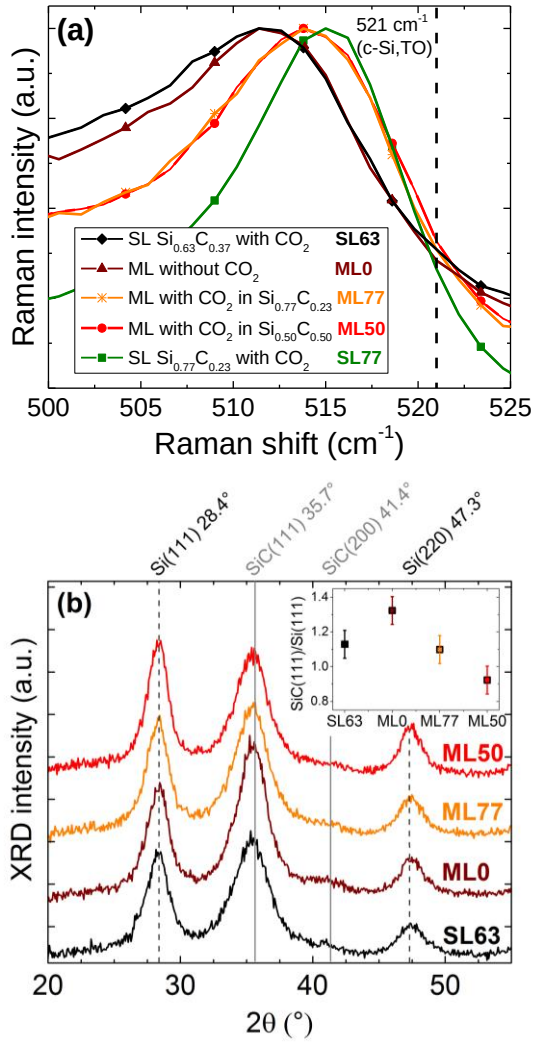

Fig. 3. Raman spectra (a) and GIXRD patterns (b) of ML with CO_2 (red) and without CO_2 (brown) annealed for 30min@1100°C by FA.

other samples. Raman results (not shown here) also prove that the Si crystallinity in $Si_{0.77}C_{0.23}$ SL samples is not influenced by the O content in the layers. This is also true for the $Si_{0.63}C_{0.37}$ SL sample with and without CO_2. In Fig. 2(a) the SL63 sample clearly shows a smaller c-Si fraction than the SL77 sample. These results are not surprising so far. However, the comparison of ML0 and ML50/ML77 is still surprising as the ML0 shows a very similar c-Si peak at exactly the same peak position as the c-Si peak of SL63. This supports the assumption from Fig. 1 suggesting strong sublayers intermixing in the ML and therefore a behavior of ML0 after annealing which is quite similar to the properties of SL63 after annealing. Finally the Raman spectra of ML50 (red, ●) and ML77 (orange, ✳) are reviewed. The shape of the c-Si Raman modes and the peak positions lie between that of the ML0 and the SL77. This is an indication for a larger c-Si fraction in ML with CO_2 compared to ML without CO_2. A higher c-Si fraction requires a local Si concentration in the samples, which is higher than 63%. This strengthens the initial assumption that the O incorporation into the ML hinders sublayer intermixing.

In Fig. 2(b) the GIXRD pattern for all samples from Fig. 2(a) are depicted, except for SL77. At first sight, all GIXRD pattern look quite similar. However, the SiC(111)/Si(111) peak intensity ratios show significant differences as depicted in the inset of Fig. 2(b). The increase of SiC(111)/Si(111) for ML0 compared with SL63 could result from a slight difference in overall Si content in these two layers and will not be discussed further. Here the difference of the three ML will be examined. SiC(111)/Si(111) shows its highest value for ML0, decreases for ML77, and decreases further for ML50. This shows that O incorporation improved the c-Si to c-SiC ratio, either by the reduction of SiC crystallinity or by the increase of c-Si phase. It can be concluded that the Si-C bond density decreases starting with ML0 over ML77 down to the lowest value for ML50 from FTIR measurements (not shown here). As mentioned before, no clear statement about the SiC crystallinity is possible.

It seems to play a subordinated role if CO_2 is added to the $Si_{0.77}C_{0.23}$ or to the $Si_{0.50}C_{0.50}$ sublayers in the ML stack. It was just argued that the majority of the Si-O bonds are formed prior to annealing. Perhaps diffusion of the unbound O from the $Si_{0.50}C_{0.50}$ to the $Si_{0.77}C_{0.23}$ layers occurs during annealing. Di Ventra *et al.* [13] calculated that the activation energy for diffusion of a single O atom in 3C-SiC is only 1.7 eV, compared to 2.5 eV in bulk Si. However, it is doubtful if these values apply for $Si_{0.50}C_{0.50}$ compared to $Si_{0.77}C_{0.23}$ layers. The second possible reason is the deposition process itself. The regulation of the CO_2 flux at the PECVD tool is much slower than the regulation of the other precursor gases. As the deposition of a single sublayer takes less than 50 s, it is assumed that there is a certain amount of CO_2 molecules in the plasma during the whole process, leading to an incorporation of O in the whole ML samples.

Combining FTIR, GIXRD and Raman results, it can be concluded that from ML0 to ML77 the c-Si phase increases, whereas the c-SiC phase decreases due to the O incorporation.

For ML50, the c-SiC phase decreases further whereas the c-Si phase stays unchanged. The decrease in c-SiC phase is probably due to the competition between Si-O and Si-C bonds. The increase of c-Si phase due to O incorporation is probably due to an already mentioned hindering effect of O on Si diffusion. Therefore, the local Si density in the ML stays higher during annealing than without O and more c-Si phase forms - probably in the form of larger Si NC. However, this difference in Si NC size stays an assumption because it is too small to be proven experimentally. The second possible explanation for an increased c-Si phase could be a higher number of Si NC in ML with O, perhaps because the incorporated O acts as a nucleation seed.

The promising results of ML surviving the annealing step due to O incorporation will be investigated further by a sublayer thickness variation to examine if size control can be achieved by this method. Additionally, transmission electron microscopy measurements should be conducted to verify the maintenance of the ML and to show the Si NC size distribution.

IV. Summary

Usually, Si NC/SiC ML structures show strong intermixing during the annealing step and are therefore not suitable for Si NC size control. In this work it is shown that the intermixing in the ML structure can be reduced by oxygen (O) incorporation during deposition. Furthermore, the formation of Si-O bonds and the increase of c-Si to c-SiC phase were observed. Although there is not enough data so far to prove that these changes of the ML with the help of O is accompanied by Si NC size control, by Si NC surface passivation, and by quantum confinement, this approach promises to fulfill those demands and will therefore be pursued further.

References

[1] F. Meillaud, A. Shah, C. Droz, E. Vallat-Sauvain, and C. Miazza, "Efficiency limits for single-junction and tandem solar cells," *Sol. Energ. Mat. Sol. Cells*, vol. 90, no. 18-19, pp. 2952–2959, 2006.

[2] G. Conibeer *et al.*, "Silicon nanostructures for third generation photovoltaic solar cells," *Thin Solid Films*, vol. 511-2, pp. 654–662, 2006.

[3] C.-W. Jiang and M. A. Green, "Silicon quantum dot superlattices: Modeling of energy bands, densities of states, and mobilities for silicon tandem solar cell applications," *J. Appl. Phys.*, vol. 99, no. 11, p. 114902, 2006.

[4] C. Summonte *et al.*, "Silicon nanocrystals in carbide matrix," *Sol. Energ. Mat. Sol. Cells*, vol. 128, pp. 138–149, 2014.

[5] K. Ding *et al.*, "Annealing induced defects in SiC, SiO_x single layers, and SiC/SiO_x hetero-superlattices," *Phys. Status Solidi A*, published online, 2012.

[6] D. Song *et al.*, "Structural characterization of annealed Si(1-x)C(x)/SiC multilayers targeting formation of Si nanocrystals in a SiC matrix," *J. Appl. Phys.*, vol. 103, p. 83544, 2008.

[7] M. Zacharias *et al.*, "Thermal crystallization of amorphous Si/SiO2 superlattices," *Appl. Phys. Lett.*, vol. 74, no. 18, pp. 2614–2616, 1999.

[8] C. Weiss, M. Schnabel, A. Reichert, P. Löper, and S. Janz, "Structural and optical properties of silicon nanocrystals embedded in silicon carbide: Comparison of single layers and multilayer structures," *Appl. Surf. Sci.*, vol. 351, pp. 550–557, 2015.

[9] C. Summonte *et al.*, "Growth and characterization of Si nanodot multilayers in SiC matrix," in *23rd European Photovoltaic Solar Energy Conference: Proceedings*, 2008, pp. 730–733.

[10] M. Schnabel *et al.*, "Absorption and emission of silicon nanocrystals embedded in SiC: Eliminating Fabry-Pérot interference," *J. Appl. Phys.*, vol. 117, no. 4, p. 45307, 2015.

[11] Y. Kurokawa, S. Yamada, S. Miyajima, A. Yamada, and M. Konagai, "Effects of oxygen addition on electrical properties of silicon quantum dots/amorphous silicon carbide superlattice," *Curr. Appl. Phys.*, vol. 10, no. 3, S435–S438, 2010.

[12] H. Guenzler and H. M. Heise, *IR-Spektroskopie*, 3rd ed. Weinheim: VCH Verlagsgesellschaft, 1996.

[13] M. Di Ventra and S. T. Pantelides, "Atomic-Scale Mechanisms of Oxygen Precipitation and Thin-Film Oxidation of SiC," *Phys. Rev. Lett.*, vol. 83, no. 8, pp. 1624–1627, 1999.